Chemical Geology 513 (2019) 153–166

Contents lists available at ScienceDirect

Chemical Geology

journal homepage: www.elsevier.com/locate/chemgeo

The ion microprobe as a tool for obtaining strontium isotopes in magmatic plagioclase: A case study at Okataina Volcanic Centre, New Zealand☆

May Sas[a,*], Noriyuki Kawasaki[b], Naoya Sakamoto[c], Phil Shane[a], Georg F. Zellmer[d], Adam J.R. Kent[e], Hisayoshi Yurimoto[b,c]

[a] School of Environment, University of Auckland, Private Bag 92019, Auckland 1142, New Zealand
[b] Natural History Sciences, Hokkaido University, Sapporo 060-0810, Japan
[c] Isotope Imaging Laboratory, Creative Research Institution, Hokkaido University, Sapporo 001-0021, Japan
[d] Volcanic Risk Solutions, Massey University, Private Bag 11222, Palmerston North 4442, New Zealand
[e] College of Earth, Ocean, and Atmospheric Sciences, Oregon State University, Corvallis, OR 97330, USA

ARTICLE INFO

Editor: Donald Porcelli

Keywords:
Sr isotopes
SIMS
Plagioclase
Okataina
Rhyolite

ABSTRACT

We investigated the potential of multi-collector secondary ion mass spectrometry (MC-SIMS) as a tool for obtaining Sr isotopic compositions in plagioclase, a ubiquitous mineral in igneous rocks that serves as a recorder of crystallization history. MC-SIMS allows for high spatial resolution analysis (~12 μm in this study) of isotopes, and therefore improves the temporal scale at which fluctuations in crystallization conditions can be recognized, ultimately improving our understanding of rates of magmatic processes. Plagioclase crystals from two young rhyolitic deposits from two major eruptive complexes, Tarawera and Haroharo, of the Okataina Volcanic Centre in New Zealand were analysed. Results were corrected for matrix effects using linear modelling of MC-SIMS data versus An contents, as well as $^{87}Sr/^{86}Sr$ ratios acquired via laser ablation inductively-coupled plasma mass spectrometry (LA-MC-ICP-MS). Corrected MC-SIMS Sr isotopic ratios had an average 2σ uncertainty of ± 0.0008 per spot, and were homogeneous in Okataina plagioclase at high spatial resolutions. Average LA-MC-ICP-MS $^{87}Sr/^{86}Sr$ ratios of plagioclase from both intra-caldera volcanic complexes (Tarawera $^{87}Sr/^{86}Sr$ = 0.7056 and Haroharo $^{87}Sr/^{86}Sr$ = 0.7054) suggest similar magma sources and similar assimilation and fractional crystallization processes for the two complexes. Overall homogeneity of plagioclase (excluding relict cores) indicates no significant changes in contributions (i.e., crustal assimilation, mafic influx) to the system during the majority of plagioclase crystal growth. Furthermore, lack of $^{87}Sr/^{86}Sr$ ratio fluctuations in plagioclase rims suggest interaction between the resident silicic magma and the intruding mafic magma that triggered the eruptions was largely limited to volatile and heat transfer. Using appropriate standards and analysis, this MC-SIMS method can be used to detect short-lived, open-system events in magma reservoirs where differences in $^{87}Sr/^{86}Sr$ isotopic ratios are significant.

1. Introduction

Analyses of micro-geochemical growth zones in individual crystals are used to understand the evolution of magmatic systems (e.g., Davidson et al., 2007, 1998; Ramos and Tepley, 2008). Crystal growth patterns are utilized to trace changes in intensive parameters (e.g., pressure, temperature, oxygen fugacity) and physio-chemical processes (e.g., fractionation, mixing) that magmas undergo as they ascend and stall in the Earth's crust before erupting at the surface. Plagioclase is one of the more frequently studied minerals because it is stable across a wide range of pressures, temperatures and H_2O contents, and responds readily to fluctuations in these conditions, ultimately providing a record of magmatic evolution (e.g., Ginibre et al., 2007; Ginibre and Davidson, 2014; Humphreys et al., 2006; Shane, 2015; Singer et al., 1995; Streck, 2008; Ustunisik et al., 2014). Plagioclase has been frequently used in petrologic studies over the last two decades, particularly with the development of techniques that permit micro-analysis of geochemical characteristics and Sr isotopic compositions in this mineral (e.g., Borges et al., 2014; Charlier et al., 2008; Christensen et al., 1995; Davidson et al., 2001; Font et al., 2008; Lange et al., 2013; Ramos et al., 2004; Takahashi et al., 2006; Tepley et al., 2000). Coupling elemental and textural zoning with $^{87}Sr/^{86}Sr$ isotopic variations in plagioclase helps in

☆ Declaration of interest: none.

* Corresponding author.
E-mail address: msas481@aucklanduni.ac.nz (M. Sas).

https://doi.org/10.1016/j.chemgeo.2019.03.016
Received 31 July 2018; Received in revised form 8 March 2019; Accepted 11 March 2019
Available online 15 March 2019

determining the degree of crustal contamination of magmas and identifying the occurrence of magmatic recharge events.

Conventional techniques utilized to determine $^{87}Sr/^{86}Sr$ isotopic compositions in plagioclase include thermal ionization mass spectrometry (TIMS) and laser ablation multi-collector inductively-coupled plasma mass spectrometry (LA-MC-ICP-MS). TIMS is a high-precision technique (with typical 2σ uncertainties of ca. 0.000025 ± 10; e.g., Charlier et al., 2006; Gao et al., 2015; Kimura et al., 2013; Lange et al., 2013), but involves time-consuming sample preparation, including micromilling and chemical purification, which limits the number of samples that can be prepared. LA-MC-ICP-MS, in contrast, is an in-situ technique that allows for rapid analysis of crystals with relatively minimal sample preparation, but slightly lower precision and accuracy (2σ commonly 0.000080 ± 30; e.g., Burns et al., 2015; Coote et al., 2018; Gao et al., 2015). However, the ablation diameter needed to maintain the aforementioned precision is large, at least 50 μm and often ≥100 μm in cases of lower Sr concentrations (e.g., Andrews et al., 2008; Christensen et al., 1995; Coote et al., 2018; Davidson et al., 2001; Gao et al., 2015; Kimura et al., 2013; Ramos et al., 2004; Vroon et al., 2008; Waight et al., 2002; Yang et al., 2013). This can result in analyses that cover more than one compositional domain (i.e., zone) within a crystal, which is also an issue for TIMS as microdrilling may result in removal of multiple compositional zones (minimum of 50 μm width and ≫100 μm in length; e.g., Chadwick et al., 2007; Charlier et al., 2008, 2006; Davidson and Tepley, 1997; Font et al., 2008; Lange et al., 2013; Morgan et al., 2007; Takahashi et al., 2013). Furthermore, small plagioclase crystals (< 50 μm) cannot currently be analysed in-situ (only via TIMS low blank chromatography; e.g., Ramos and Tepley, 2008), and plagioclase crystals containing abundant micro-inclusions prove challenging to analyse. In an attempt to advance our understanding of magmatic processes and minimize issues surrounding averaging of compositional domains, small crystal size, and inclusion-rich crystals, we utilized a multi-collector secondary ion mass spectrometer (MC-SIMS) to obtain high resolution (~12 μm diameter) $^{87}Sr/^{86}Sr$ isotopic compositions in plagioclase. The ~12 μm spatial resolution of MC-SIMS for Sr isotopes is unobtainable by TIMS and LA-MC-ICP-MS since such small amounts of sample do not contain enough Sr for high-precision analysis (Charlier et al., 2006; Ramos and Tepley, 2008).

The ion microprobe allows for in-situ high resolution, high sensitivity analysis with spatial resolution on a micron scale and analytical precision better than 0.001 depending on the material and isotope species analysed (e.g., Budd et al., 2017; Kawasaki et al., 2017, 2015; Valley and Kita, 2009; Weber et al., 2005). Another advantageous aspect of SIMS is the ability to overcome many isobaric interferences through use of high mass resolving power ($M/\Delta M$). Ion microprobe analysis of Sr isotopes has been conducted (Exley, 1983; Kennedy et al., 1990; Sano et al., 2008; Scatena-Wachel, 1986; Weber et al., 2005), although previous studies have focused on carbonates (Table 1), particularly calcite, as it is compositionally simple and has high abundances of Sr yet low Rb/Sr (thus minimizing ^{87}Rb interferences on ^{87}Sr). Here we attempt to obtain accurate $^{87}Sr/^{86}Sr$ data of plagioclase, a compositionally more complex mineral with higher Rb/Sr ratios. In this study, instrument configuration, isobaric interferences, results, geochemical implications, and applicability of the ion microprobe as means for measuring Sr isotopic composition in plagioclase are discussed.

2. Okataina Volcanic Centre and sample selection

Plagioclase crystals used for this study were collected from the Okataina Volcanic Centre (OVC) in the Taupo Volcanic Zone (TVZ; Fig. 1). The TVZ is a NNE-SSW trending active volcanic arc in North Island, New Zealand, and is the on-land continuation of the Tonga-Kermadec arc, where volcanism is associated with subduction of the Pacific Plate beneath the Australian Plate (Stern, 1987). Formation of the TVZ started ca. 2 Ma ago with regular episodic volcanic activity resulting in total erupted volume > 10^4 km^3, which is comparable to the Yellowstone system in North America, making it the most active Quaternary silicic system on Earth (Houghton et al., 1995; Wilson et al., 1984). The OVC is one of only two currently dormant rhyolite centres in the central TVZ, and of the two is the most recently active. Voluminous, regular activity at OVC began at ca. 625 ka and includes at least three caldera-forming events (Cole et al., 2014). Volcanism at OVC is bimodal with dominantly rhyolitic and minor basaltic erupted material (Nairn, 2002). Studies of rhyolitic deposits indicate that many OVC eruptions, both caldera-forming and intra-caldera, result from influx of hotter mafic magma into cooler, multi-level and laterally discontinuous silicic reservoirs (e.g., Leonard et al., 2002; Nairn et al., 2004, 2005, 2001; Shane, 2015; Shane et al., 2008; Storm et al., 2014, 2012, 2011).

There are two intra-caldera volcanic complexes at OVC with distinctive and parallel linear vent alignments, Tarawera to the south and Haroharo to the north. Eruptions at both complexes emanate from multiple vents along the length of their respective linear vent zones, a characteristic that is atypical for silicic eruptions and is thought to be controlled by regional extensional structures (Nairn, 2002). Selected units for analysis here include pumice from two recent post-caldera eruptions: (1) Kaharoa (0.7 ka), which erupted from the Tarawera Volcanic Complex, and (2) Rotoma (9.5 ka), which erupted from the Haroharo Volcanic Complex (Nairn, 2002). Both units reflect typical post-50 ka OVC eruptive behaviour (i.e., explosive and effusive, simultaneous ejection from multiple vents, eruption of more than one magma composition; e.g., Shane et al., 2008, 2007; Smith et al., 2006). Their mineralogy (plagioclase + quartz ≫ Fe-Ti oxides > orthopyroxene + hornblende) is also typical of recently erupted magmas, although Kaharoa contains biotite and minor cummingtonite, whereas in Rotoma cummingtonite is a major ferromagnesian mineral and biotite is absent (any biotite in Rotoma is relict; Leonard et al., 2002; Nairn et al., 2004; Smith et al., 2005).

Kaharoa is the youngest rhyolitic eruption and the largest (~9 km^3) TVZ eruption in the last 1000 years, with eruptive materials including both lavas and pyroclastics with SiO_2 = 75–77 wt% (Leonard et al., 2002; Nairn et al., 2004; Sahetapy-Engel et al., 2014). The Kaharoa magmatic system has been modelled as a stratified, sill-like (8 km × 1 km, > 1 km in thickness) reservoir with three compositionally diverse and individually homogeneous rhyolitic magmas: (1) T1, the first to erupt, (2) T2, the last to erupt and with higher Zr and Sr relative to T1, and (3) T3, un-erupted rhyolite that mixed with basalt-derived residual melt (dacite) to produce erupted rhyodacites (Nairn et al., 2004). Kaharoa was specifically selected based on previous studies (Leonard et al., 2002; Nairn et al., 2004, 2001; Shane, 2015) that

Table 1
Summary of previous $^{87}Sr/^{86}Sr$ ion microprobe studies.

Instrument	Spot (μm)	Sample	Sr (ppm)	Max 2σ	M/ΔM	Study
AEI-IM20	10	Calcite	400	0.002	200	Exley (1983)
AEI-IM20	10	Calcite	400	0.002	200	Scatena-Wachel (1986)
SHRIMP-RG	25	Otolith	≤1500	0.002	7000–9000	Weber et al. (2005)
NanoSIMS NS50	5	Otolith	< 2000	0.003	3600	Sano et al. (2008)
IMS 1280HR	12	Plagioclase	< 1500[a]	0.0009	7000	This study

[a] Sr ppm for Kaharoa plagioclase from Shane (2015).

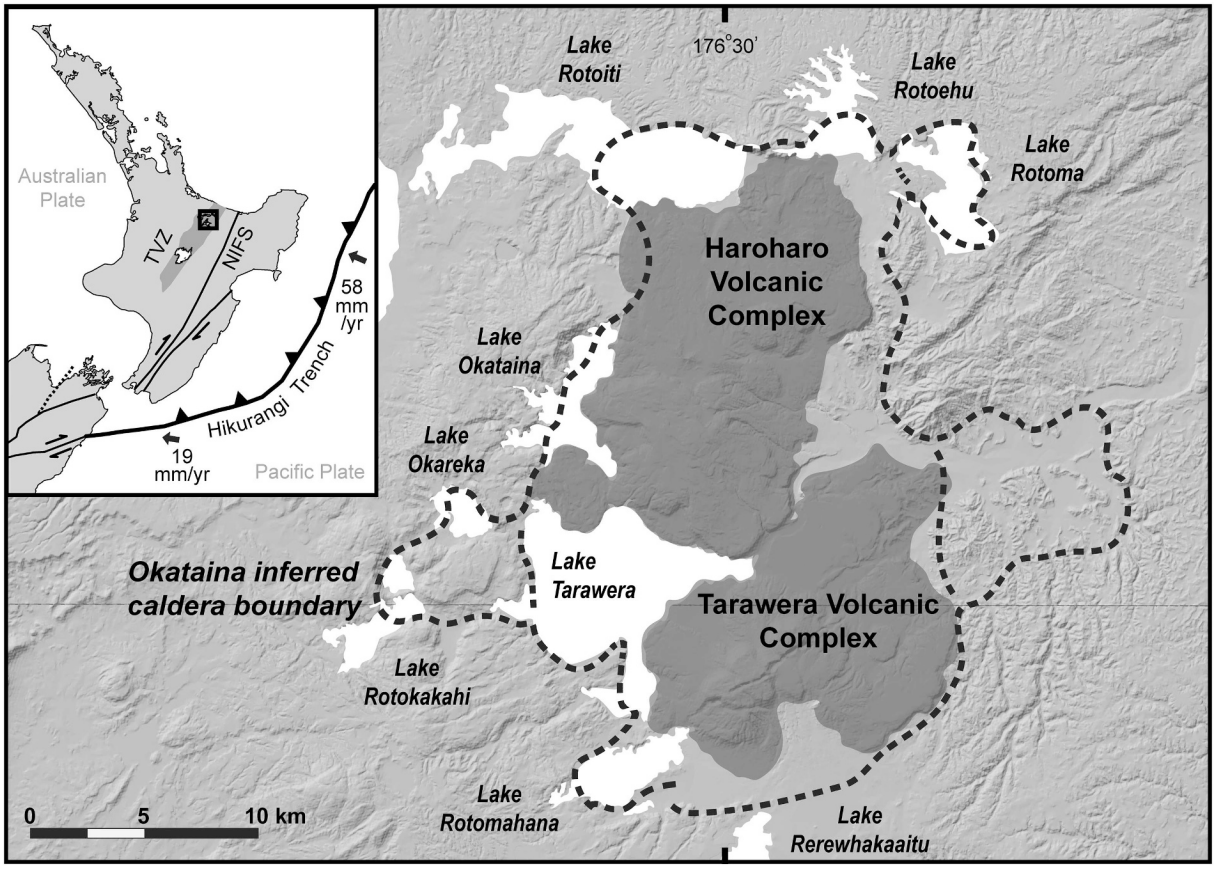

Fig. 1. Map of the Okataina Volcanic Centre (OVC) showing caldera boundaries and intra-caldera volcanic centres (modelled after Smith et al., 2006). OVC is one of two currently active silicic centres within the Taupo Volcanic Zone (TVZ; shaded region in upper left image). North Island Fault System (NIFS) shown on inset map is from Wilson and Rowland (2016). Subduction rates shown on the inset map are from Wallace et al. (2009).

suggested multiple injections of basalt into the Kaharoa sill occurred before eruption. Plagioclase used for analysis was extracted from T2, because this unit shows greater evidence for interaction with basalt than T1, as well as representing the largest volumetric component of the Kaharoa magmatic system (Nairn et al., 2004).

Rotoma also erupted pyroclastics and lavas with high silica contents (SiO_2 = 75–78 wt%) and similar volume to Kaharoa (~8 km^3; Smith et al., 2006). Smith et al. (2006) interpreted the Rotoma magmatic system to be a storage system with separate, well-homogenised bodies of magma and multiple conduits. Two compositionally discrete magmas (RT1 and RT3) were tapped during the Rotoma eruption and hybridized in central vents to form a third unit (RT2). Smith et al. (2006) suggest that Rotoma rhyolites RT1 and RT3, unlike the Kaharoa rhyolites T1 and T2, were able to homogenise rather than mingle due to them having similar H_2O contents, densities and viscosities. Although Rotoma deposits show no evidence for interaction with basalt, mafic magma intrusion remains a possible cause for eruption because this process is common at the OVC. An alternative triggering mechanism could be seismic activity, as Rotoma deposits are found directly above an earthquake rupture (Smith et al., 2006). Plagioclase crystals from unit RT2 were selected for analysis.

Additional criteria for unit selection included abundance (≥1%) and size (≥100 μm) of plagioclase crystals and availability of whole rock and mineral geochemistry data. Size criteria were set to test the accuracy of isotopic ratios using additional methods, which require large (≥100 μm) crystals. Approximately 300 plagioclase crystals from each unit were handpicked, mounted in 25 mm diameter epoxy plugs, and polished for microanalysis. Identification of compositional and textural characteristics was completed using electron backscatter imaging (BSE) and electron microprobe analysis (EPMA). Optimal crystals for isotopic microanalyses were selected based on crystal orientation, complete crystal stratigraphy from core to rim, and a good crystal surface (i.e., minimal scratches, cracks, and mineral or melt inclusions). A total of seven representative crystals were analysed from Kaharoa and five from Rotoma.

3. Analytical methods

3.1. Electron microprobe analysis

EMPA was completed to determine major and minor element concentrations of plagioclase and was done using a JEOL JXA-8230 SuperProbe at Victoria University of Wellington. EMPA analyses were done post-MC-SIMS, to match spot locations as closely as possible, and pre-LA-MC-ICP-MS. Elements analysed and their uncertainties are Si (1%), Ca (2%), Na (4%), K (7%), Al (1%), Mg (4%), and Fe (5%). The precision reported here is calculated using standard values collected during the analytical session. In effort to help reduce uncertainties, Mg and Fe had peak counting times of 90 s, whereas all other elements have peak counting times of 30 s. However, for concentrations close to the detection limit, such as Mg in plagioclase, uncertainties will be larger. Instrument conditions included an accelerating voltage of 15 kV, 1–2 μm beam size, and a 20 nA current. NMNH-115900 plagioclase was used as a standard.

3.2. Laser ablation multi-collector inductively-coupled plasma mass spectrometry analysis

MC-SIMS $^{87}Sr/^{86}Sr$ ratios measured in OVC plagioclase were compared to $^{87}Sr/^{86}Sr$ ratios obtained from LA-MC-ICP-MS. Analyses were

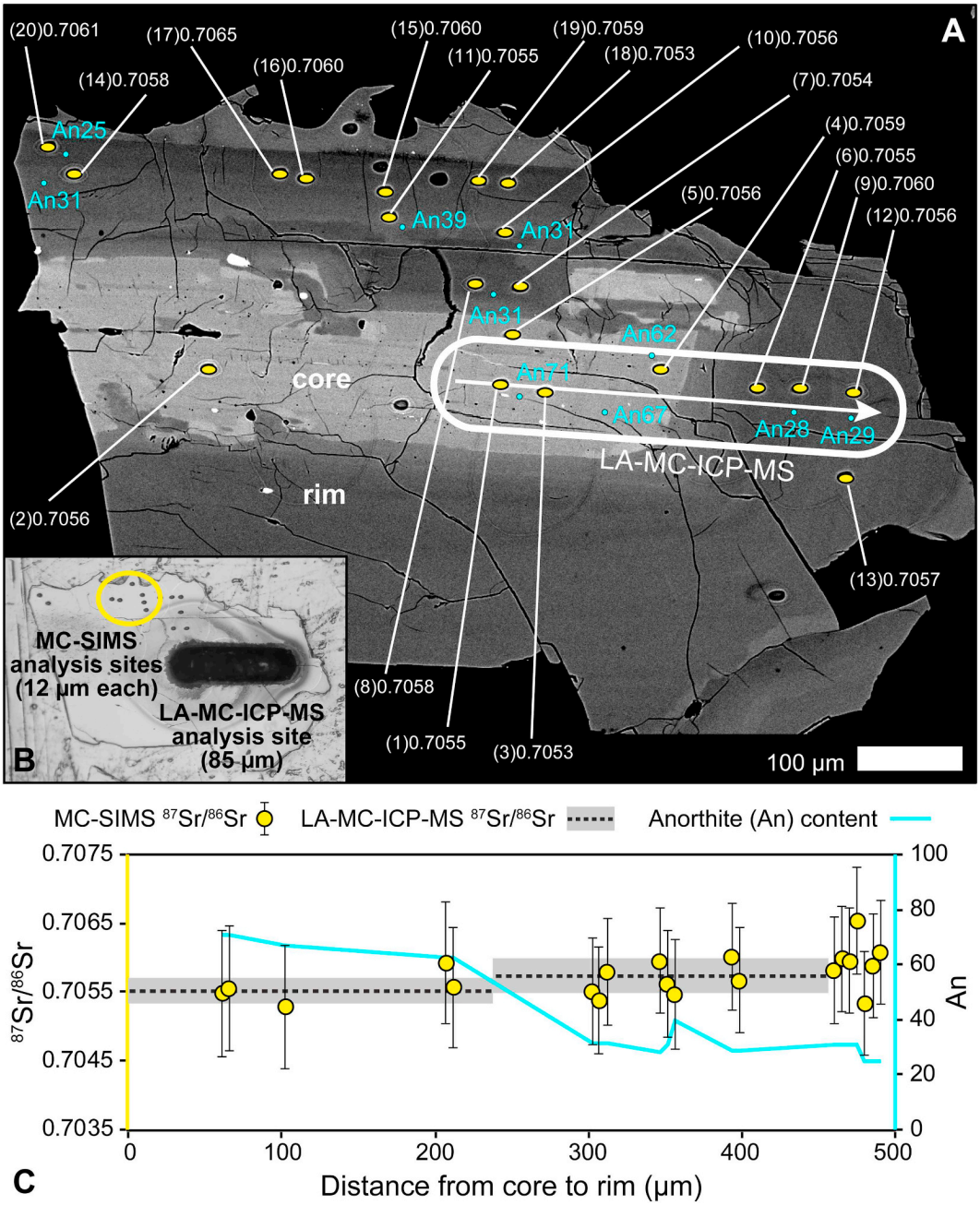

Fig. 2. (A) An annotated BSE image of a Kaharoa plagioclase crystal showing the locations of MC-SIMS analytical sites (yellow spots), the LA-MC-ICP-MS trough (white oval with arrow indicating direction of analysis), and EMPA analytical sites with their respective An contents (blue spots and text). The straight white lines and adjacent numbers list the specific $^{87}Sr/^{86}Sr$ ratio of the MC-SIMS analytical site they point to, and the numbers listed in parenthesis near each MC-SIMS $^{87}Sr/^{86}Sr$ ratio indicate the sequential order in which the sites are shown on the graph in part C. Distances from core-to-rim were measured along the LA-MC-ICP-MS trough. MC-SIMS sites that are not situated parallel to the LA-MC-ICP-MS trough were grouped with MC-SIMS site that are situated parallel to the trough and represent the same compositional domain (zone) within the crystal (for easier visibility, grouped MC-SIMS analyses have been plotted 5 µm apart on core-to-rim profiles). The core appears brighter relative to the rim due to higher An contents. (B) A reflected light image of the same crystal showing the relative size difference between LA-MC-ICP-MS analysis (85 µm) and ion microprobe sites (12 µm). (C) A graph illustrating the core-to-rim variability of $^{87}Sr/^{86}Sr$ ratios and An contents of the Kaharoa plagioclase crystal in part A. The yellow spots represent $^{87}Sr/^{86}Sr$ ratios of specific sites acquired via MC-SIMS, with their respective errors shown as vertical black lines. The dashed, horizontal black lines represent $^{87}Sr/^{86}Sr$ ratios acquired via LA-MC-ICP-MS for the plagioclase core and rim, and the grey envelope surrounding each dash line indicates the associated error (2se). The bright blue line represents An contents calculated using EMPA data. (For interpretation of the references to colour in this figure legend, the reader is referred to the web version of this article.)

done at the WM Keck Collaboratory for Plasma Mass Spectrometry at Oregon State University using a Nu Plasma MC-ICP-MS equipped with a Photon Machines G2 193nm ArF Excimer LA system. The carrier gas was He at flow rates of 0.3 L/min. Ablation troughs were 65–85 µm in diameter and 20–25 µm in depth (depth measured using a Keyence VK-X200 3D laser scanning microscope). Smaller ablation diameters were used in effort to analyse the same compositional domains (or as similar as possible) analysed by MC-SIMS. Laser analyses were done using a fluence of 4.84 J/cm^2 and pulse rates of 15 Hz for standards and 30 Hz for plagioclase. Troughs were analysed across samples at a rate of 5 µm/s. Measured masses were 83, 84, 85, 86, 87 and 88. On-peak corrections were made by measuring background values for Kr isotopes and other

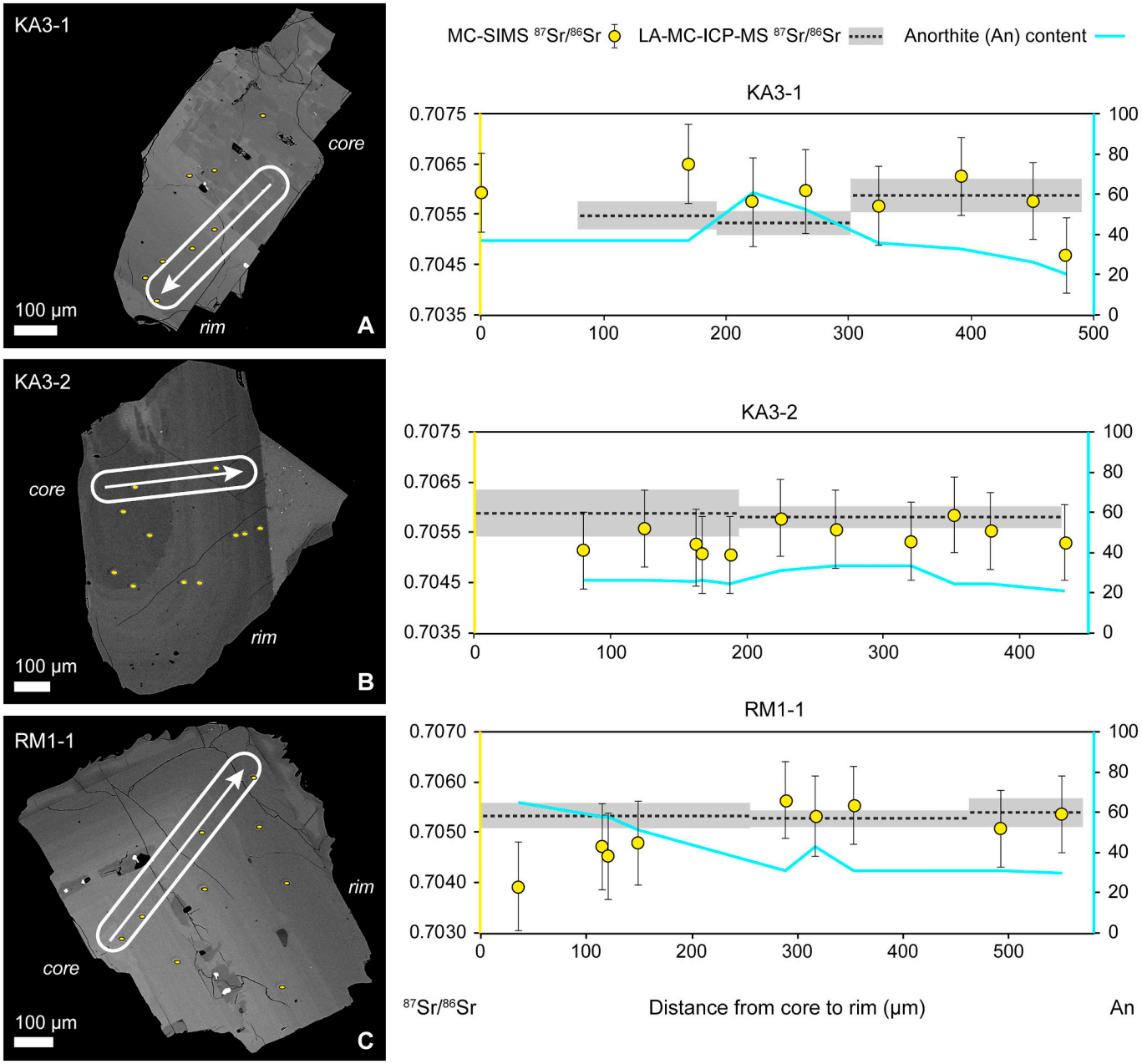

Fig. 3. BSE images of representative plagioclase crystals selected for analyses, with common zoning patterns and mineral textures. The yellow spots represent $^{87}Sr/^{86}Sr$ ratios of specific sites acquired via MC-SIMS, with their respective errors shown as vertical black lines. The dashed, horizontal black lines represent $^{87}Sr/^{86}Sr$ ratios acquired via LA-MC-ICP-MS for the plagioclase core and rim, and the grey envelope surrounding each dash line indicates the associated error (2se). The bright blue line represents An contents calculated using EMPA data. (A) Kaharoa crystal with boxy-cellular texture in the core. (B) Kaharoa crystal with a distinct and frayed transition from a sodic core to a calcic rim. (C) Rotoma crystal exhibiting gradual decrease in An contents from core to rim, as well as a zone with inclusions between core and rim. (For interpretation of the references to colour in this figure legend, the reader is referred to the web version of this article.)

gas species introduced by the plasma prior to ablation of samples, then subtracting the background values from measured intensities. Corrections for mass bias were applied using measured $^{86}Sr/^{88}Sr = 0.1194$. Contributions from ^{87}Rb were corrected for by measuring ^{85}Rb intensity, and calculated ^{87}Rb contributions used the same mass bias as calculated for Sr isotopes. Previous studies have shown that contributions from Ca dimers and argides are negligible (Miller and Kent, 2009), therefore Ca species were not monitored. NIST 610 glass was used for tuning the instrument, and a modern gastropod ($^{87}Sr/^{86}Sr$ 0.709190 ± 0.000008; Miller and Kent, 2009) was used as an internal standard. A correction was applied to measured $^{87}Sr/^{86}Sr$ ratios in plagioclase based on small differences between the measured and accepted composition of the gastropod during the same analytical session (typically $\Delta^{87}Sr/^{86}Sr$ of 0.0002 to 0.0004; Miller and Kent, 2009). A secondary standard, a low-Rb, high-Sr clinopyroxene with homogeneous $^{87}Sr/^{86}Sr$ (0.704470 ± 0.000017 and 0.704482 ± 0.000010; Burns et al., 2015), was analysed as an unknown to further monitor instrument accuracy. The average $^{87}Sr/^{86}Sr$ value for the clinopyroxene standard throughout measurement was 0.70463 ± 0.00017. The average $^{84}Sr/^{86}Sr$ ratio measured of this standard was 0.0569 ± 0.0014.

Troughs were set up from core to rim of each crystal to measure $^{87}Sr/^{86}Sr$ compositional profiles similar to those obtained via MC-SIMS (see Section 3.3; e.g., Figs. 2–3). Plagioclase signals were divided and reduced into core, middle and rim bins, or into core and rim bins when the crystal was compositionally homogeneous and/or when more bins

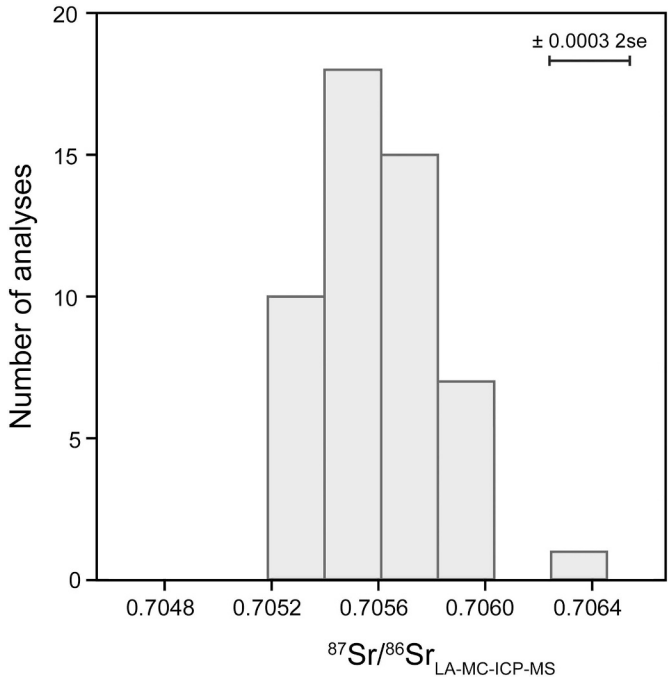

Fig. 4. Histogram depicting LA-MC-ICP-MS $^{87}Sr/^{86}Sr$ ratios in OVC plagioclase. Individual (per crystal) ratios and respective errors are included in Figs. 2–3 and 5–6, and are listed in Table 2.

were not statistically viable. These bins were selected in an effort to match the spatial resolution of MC-SIMS, as well as to track $^{87}Sr/^{86}Sr$ variations between zones with differing An contents. Reported uncertainties in LA-MC-ICP-MS $^{87}Sr/^{86}Sr$ ratios represent standard error (2se) calculated from repeat analysis of the measured $^{87}Sr/^{85}Sr$ ratios in the selected portion of each crystal, propagated quadratically with the standard error calculated from repeated analysis of the gastropod standard for that analytical session (to include both the within-run uncertainty and external uncertainty). To account for any inclusions sampled by the laser during ablation, signals showing ^{85}Rb spikes were excluded during the reduction process.

3.3. Secondary ion mass spectrometry analysis

Measurements of $^{87}Sr/^{86}Sr$ isotopic compositions in plagioclase were done using a CAMECA IMS 1280-HR located at Hokkaido University. An $^{16}O^-$ primary ion beam of 23 keV with a current of ~6 nA and a diameter of ~12 μm was used in the experiment. The mass resolution of $M/\Delta M$ was set at ~7000 to maintain sub-per mille precision. While many interferences are eliminated through use of $M/\Delta M \geq 7000$ (Weber et al., 2005), several Ca species are still potentially problematic, and isobaric interference of $^{87}Rb^+$ is unresolvable (respective $M/\Delta M$):

$^{87}Sr^+$: $^{87}Rb^+$ (300,000), $^{43}Ca^{44}Ca^+$ (16,200), $^{48}Ca^{39}K^+$ (11,800), $^{86}Sr^1H^+$ (10,600)
$^{86}Sr^+$: $^{42}Ca^{44}Ca^+$ (17,800), $^{40}Ca^{46}Ca^+$ (12,200), $^{43}Ca_2{}^+$ (10,400)

Therefore contributions of $^{87}Rb^+$ on $^{87}Sr^+$ were corrected based on secondary ion intensity of $^{85}Rb^+$ (Fig. A1; Table B1) assuming $^{85}Rb/^{87}Rb = 2.5926$ (Rosman and Taylor, 1998). Contributions of $^{42}Ca^{44}Ca^+$ on $^{86}Sr^+$ and $^{43}Ca^{44}Ca^+$ on $^{87}Sr^+$ were corrected based on $^{40}Ca_2{}^+$ and assuming that secondary ion intensities of the Ca dimers equal to Ca-isotope ratios of $^{40}Ca/^{42}Ca = 149.8145$, $^{40}Ca/^{43}Ca = 702.3913$, and $^{40}Ca/^{44}Ca = 46.3115$ (Rosman and Taylor, 1998), although the contributions of the Ca dimer ions were determined to be negligible in our analyses (Fig.A2; Table B1). Contributions of $^{86}Sr^1H^+$ were evaluated using $M/\Delta M$ = ca. 20,000 and deemed to be trivial (Fig. A2). Positive secondary ions ($^{85}Rb^+$, $^{86}Sr^+$, and $^{87}Sr^+$) were measured simultaneously in multi-collection mode using three electron multipliers (EMs). Obtained count rates were corrected for EM dead time and relative yield of each detector. Each measurement was conducted with 100 cycles of counting the secondary ions for 4 s. On spots analysed using multi-collection mode, $^{40}Ca_2{}^+$ was subsequently measured with 10 cycles of counting for 4 s using an EM by the peak-jumping of a sector magnet. Plagioclase (anorthite, $An_{97–94}$, mounted and polished) from Miyakejima volcano, Japan, with homogeneous $^{87}Sr/^{86}Sr$ (0.70345; Arakawa et al., 1992; Kimura et al., 2013) was used as a calibration standard to normalize differences in the relative yield of detectors between each analytical session with average external reproducibility of 0.0007 (2σ). Approximately 35% of analyses comprised of standard measurements.

4. Results

4.1. Plagioclase composition and textures

Major and minor element concentrations of plagioclase are summarized in Table B2. Plagioclase An contents are similar across the two Okataina units, and the majority of crystals exhibit normal zoning. Kaharoa plagioclase is in the range $An_{20–43}$ with few $An_{60–71}$ cores.

Table 2
LA-MC-ICP-MS analyses of OVC plagioclase.

Plagioclase	Bin	$^{87}Sr/^{86}Sr$	2se	Plagioclase	Bin	$^{87}Sr/^{86}Sr$	2se
Kaharoa				Rotoma			
KA2-1	Core	0.70547	0.00030	RM1-1	Core	0.70534	0.00026
	Mid	0.70538	0.00015		Mid	0.70528	0.00016
KA2-2	Core	0.70552	0.00019		Rim	0.70540	0.00028
	Rim	0.70574	0.00025	RM1-2	Core	0.70583	0.00027
KA2-3	Core	0.70635	0.00038		Rim	0.70558	0.00018
	Mid	0.70602	0.00081	RM1-5	Core	0.70569	0.00033
	Rim	0.70537	0.00046		Mid	0.70556	0.00020
KA2-4	Mid	0.70549	0.00022		Rim	0.70569	0.00025
	Rim	0.70526	0.00034	RM2-1	Core	0.70597	0.00035
KA3-1	Core	0.70549	0.00028		Mid	0.70570	0.00019
	Mid	0.70534	0.00023		Rim	0.70559	0.00018
	Rim	0.70589	0.00033	RM3-1	Core	0.70580	0.00032
KA3-2	Core	0.70590	0.00047		Mid	0.70569	0.00017
	Rim	0.70581	0.00021		Band	0.70593	0.00026
KA3-6	Core	0.70550	0.00041		Rim	0.70570	0.00022
	Mid	0.70558	0.00022				
	Rim	0.70568	0.00043				

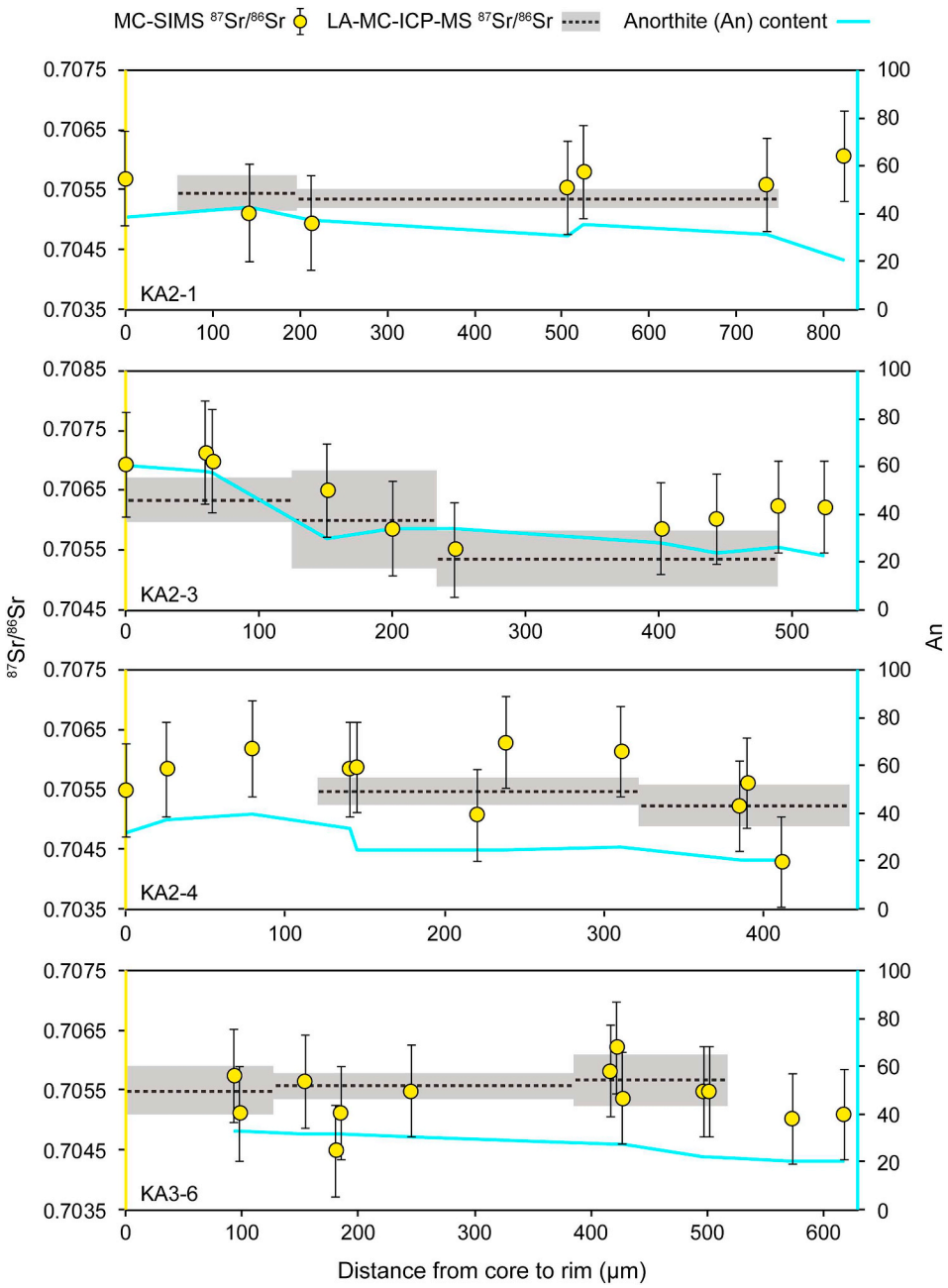

Fig. 5. Graphs illustrating the core-to-rim variability of $^{87}Sr/^{86}Sr$ ratios and An contents of Kaharoa plagioclase. The yellow spots represent $^{87}Sr/^{86}Sr$ ratios of specific sites acquired via MC-SIMS, with their respective errors shown as vertical black lines. The dashed, horizontal black lines represent $^{87}Sr/^{86}Sr$ ratios acquired via LA-MC-ICP-MS for the plagioclase core and rim, and the grey envelope surrounding each dash line indicates the associated error (2se). The bright blue line represents An contents calculated using EMPA data. (For interpretation of the references to colour in this figure legend, the reader is referred to the web version of this article.)

Rotoma plagioclase is in the range $An_{29–43}$ with few calcic cores or compositional zones with $An_{48–65}$. Contents of FeO in all plagioclase crystals mimic An compositional patterns (decrease with lower An). Plagioclase crystals from the two units also have resorbed cores that are either more or less calcic than their respective rim. Calcic cores have either a sharp (Fig. 2) or gradational (Fig. 3C) boundary with sodic rims, whereas sodic cores are rounded (and often frayed-looking; Fig. 3B) with calcic rims. In both units, the differences in An contents between sodic cores and calcic rims are lesser than between calcic cores and sodic rims. Several Kaharoa crystals exhibit boxy-cellular core textures (Fig. 3A) that resemble chess boards, as noted by Shane (2015). Rotoma crystals rarely exhibit boxy-cellular textures, but several crystals have distinct zones (≤80 μm in width) between the core and rim that are dominated by inclusions (Fig. 3C).

4.2. LA-MC-ICP-MS analyses

Inter- and intra-crystal Sr isotopic compositions of plagioclase are commonly homogeneous within error based on LA-MC-ICP-MS analysis. LA-MC-ICP-MS results are summarized in Fig. 4 and listed in Table 2. Kaharoa (Figs. 2–3 and 5) and Rotoma (Figs. 3 and 6) crystals cluster within the same $^{87}Sr/^{86}Sr$ range. Plagioclase crystals analysed in this study show no clear correlation between An contents and Sr isotopic compositions.

4.3. MC-SIMS analyses

Raw MC-SIMS data (corrected for $^{87}Rb^{+}$ and Ca dimers, see Section 3.3) were corrected in two steps: (1) An instrumental mass fractionation

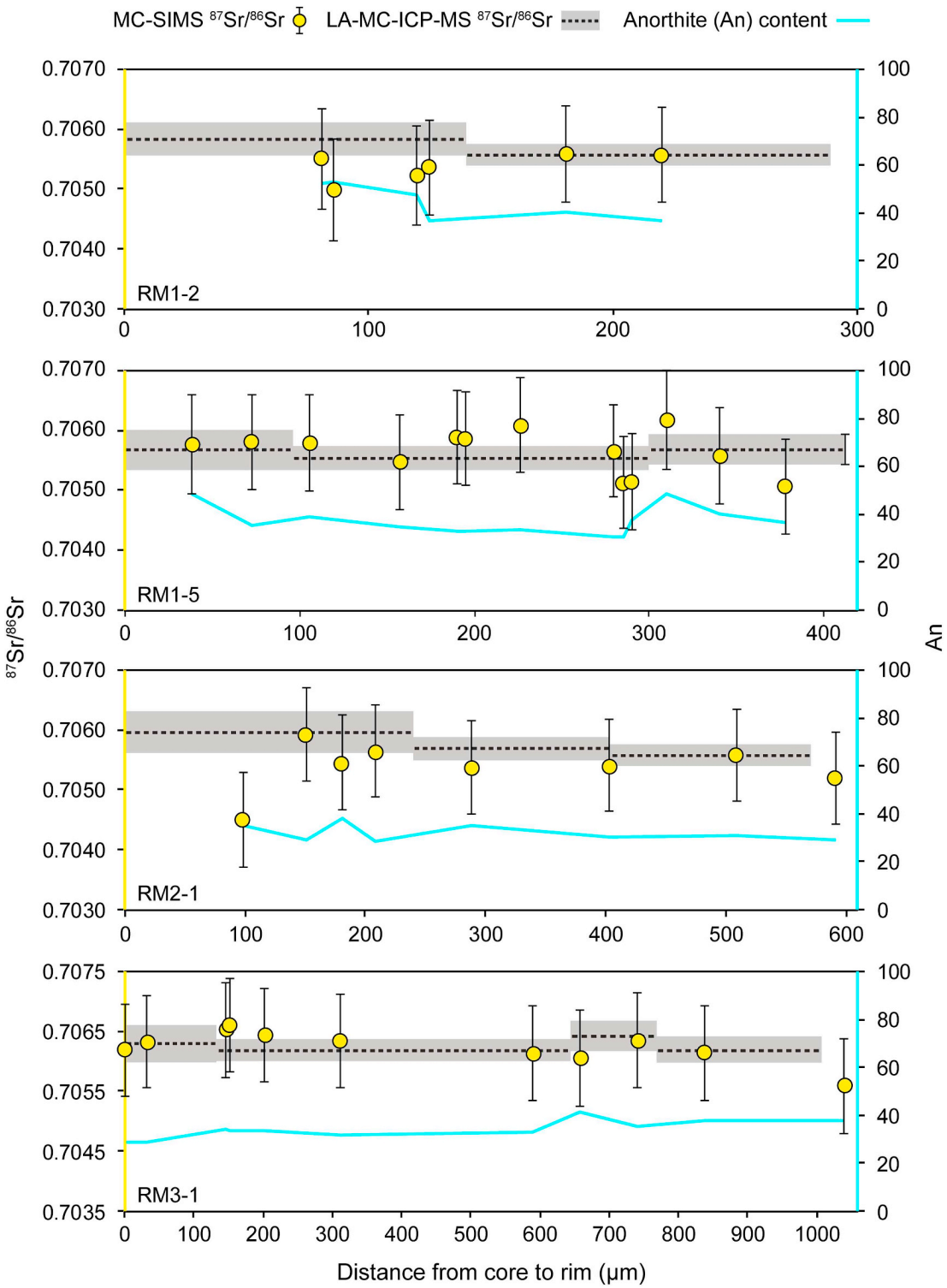

Fig. 6. Graphs illustrating the core-to-rim variability of $^{87}Sr/^{86}Sr$ ratios and An contents of Rotoma plagioclase. The yellow spots represent $^{87}Sr/^{86}Sr$ ratios of specific sites acquired via MC-SIMS, with their respective errors shown as vertical black lines. The dashed, horizontal black lines represent $^{87}Sr/^{86}Sr$ ratios acquired via LA-MC-ICP-MS for the plagioclase core and rim, and the grey envelope surrounding each dash line indicates the associated error (2se). The bright blue line represents An contents calculated using EMPA data. (For interpretation of the references to colour in this figure legend, the reader is referred to the web version of this article.)

(IMF) correction was applied (annotated as $^{87}Sr^{+}/^{86}Sr^{+}_{SIMS}$ in the equation below). Raw and IMF-corrected $^{87}Sr^{+}/^{86}Sr^{+}$ ratios are listed in Table B1. (2) A matrix effect correction was made, because MC-SIMS data show a broad correlation between SIMS $^{87}Sr^{+}/^{86}Sr^{+}$ secondary ion intensity ratios and plagioclase An contents (Fig. 7). The complexity of plagioclase, a solid solution series of Ca–Na feldspar minerals, makes it a likely candidate for an analytical matrix effect – a well-known issue with SIMS analysis (e.g., Eiler et al., 1997). Fig. 7 specifically shows that higher An zones yield higher $^{87}Sr^{+}/^{86}Sr^{+}$ ion count ratios; a pattern that was not observed in data acquired via LA-MC-ICP-MS.

Since the Sr isotopic ratios obtained by LA-MC-ICP-MS yielded constant $^{87}Sr/^{86}Sr$ ratios for zones with uniform An contents, the

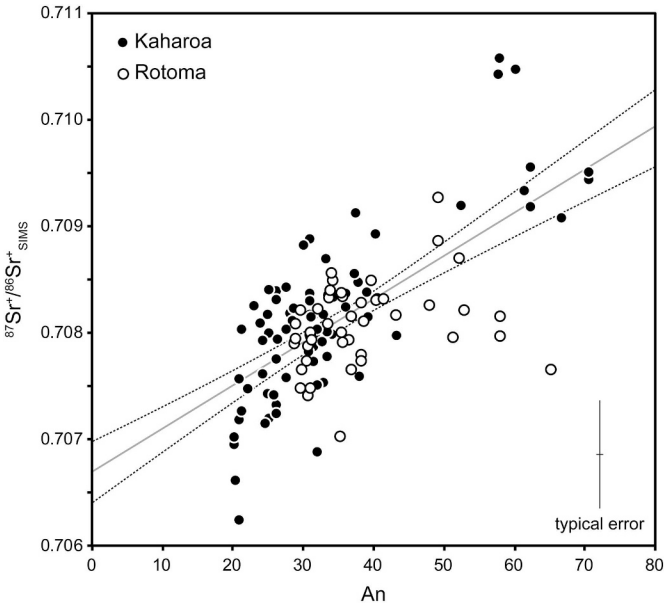

Fig. 7. Graphical representation of correlation (matrix effect) between IMF-corrected MC-SIMS $^{87}Sr^{+}/^{86}Sr^{+}$ ion intensity ratios ($^{87}Sr^{+}/^{86}Sr^{+}_{SIMS}$) and EMPA An contents in plagioclase from Kaharoa and Rotoma (Table B1). The typical error bars on the bottom right represent the 2σ reproducibility for MC-SIMS and 2σ analytical error for EMPA. The solid grey line represents linear regression of MC-SIMS data and has a slope of 4.06 (± 0.78) × 10^{-5} and a y-intercept of 0.70669 (± 0.00029). The dotted grey lines provide the 1σ error envelope. The linear regression was used to correct for the matrix effect (see Section 4.3).

observed matrix effects for SIMS data can be corrected using these LA-MC-ICP-MS data. The correction was conducted using the following equation:

$$\frac{^{87}Sr}{^{86}Sr}_{final} = \left[\left(\frac{^{87}Sr^{+}}{^{86}Sr^{+}}_{SIMS}\right) - (m \times An\ content) - \left(y - \frac{^{87}Sr}{^{86}Sr}_{LA-MC-ICP-MS}\right)\right]$$

The LA-MC-ICP-MS $^{87}Sr/^{86}Sr$ ratio used for calculations is 0.70561 ± 0.00045, and it represents the average LA-MC-ICP-MS value. Variables m and y represent the slope (4.06 × 10^{-5} ± 0.78 × 10^{-5}) and y-intercept (0.70669 ± 0.00029), respectively, calculated using the ISOPLOT (Ludwig, 2003) linear regression model 1 for all SIMS $^{87}Sr^{+}/^{86}Sr^{+}$ ion intensity ratios versus An contents (Fig. 7). We propagated the uncertainties of the repeated measurements of the Miyakejima anorthite standard, the LA-MC-ICP-MS data (2SD), and the slope and intercept of the regression, to obtain a combined precision of about ± 0.0008 (2σ) for our MC-SIMS analyses. Final, matrix effect-corrected $^{87}Sr/^{86}Sr$ ratios are listed in Table 3.

Following matrix effect correction, the Sr isotopic ratios obtained via MC-SIMS are in agreement with Sr isotopic ratios obtained through LA-MC-ICP-MS for the same crystal compositional domains within the errors. Thus, we successfully measured $^{87}Sr/^{86}Sr$ ratios for the plagioclase crystals with ± 0.0008 precision and ~12 μm spatial resolutions by MC-SIMS.

5. Discussion

5.1. Implications for using the MC-SIMS technique

MC-SIMS is potentially valuable for deciphering magmatic processes at higher spatial resolutions. The precision (± 0.0008) of the MC-SIMS method may be inadequate to identify variations in large, buffered magmatic systems in continental settings or mid-ocean ridge volcanoes, where isotopic fluctuations are slight (e.g., Lange et al., 2013; Wolff et al., 1999; Table 4). However, many studies that investigate isotopic fluctuations in volcanic crystals extracted from rocks from subduction zones, flood basalts, and intra-plate basalts reveal isotopic heterogeneities greater than the average MC-SIMS error (e.g., Alves et al., 2009; Borges et al., 2014; Burns et al., 2015; Charlier et al., 2008; Coote et al., 2018; Davidson et al., 2001; Font et al., 2008; Gao et al., 2015; Tepley et al., 2000; Yang et al., 2013; Table 4). The ion microprobe therefore allows for in-situ Sr isotopic analysis and minimal sample preparation relative to TIMS, and offers a spatial resolution that is five to ten times greater than that of LA-MC-ICP-MS.

5.2. Sr diffusion in OVC plagioclase?

Sr diffusion may have dampened any original $^{87}Sr/^{86}Sr$ variations that may have been present in OVC plagioclase. Diffusion of Sr is more rapid in sodic than in calcic plagioclase. At a temperature range of 724–760 °C (Nairn et al., 2004; Smith et al., 2006), and an An range of 20–43, diffusion coefficients range from 1.4×10^{-19} to 5.0×10^{-21} $m^2\,s^{-1}$ (Giletti and Casserly, 1994). To provide a maximum timescale for diffusion to equilibrate potential initial $^{87}Sr/^{86}Sr$ variations, we can use the approach of Zellmer et al. (1999) and assume an initial step starting profile with relative variations in ^{87}Sr and ^{86}Sr concentrations, i.e., variable $^{87}Sr/^{86}Sr$ ratios, and with a step width of 70 μm (equivalent to the average spacing of the analyses undertaken in this study). In this scenario, any isotopic variations would decay to 10% of their initial values between ca. 300 yrs. (760 °C, An_{20}) and ca. 8000 yrs. (724 °C, An_{43}). However, Shane (2015) analysed numerous Kaharoa plagioclase crystals for major, minor and trace element compositions, and showed that Sr concentration profiles mimic An trends in Kaharoa plagioclase (i.e., increasing with An contents). This observation is inconsistent with any progressed degree of Sr elemental diffusion, which would result in Sr profiles that mirror An trends (e.g., Bindeman et al., 1998; Dohmen et al., 2017; Zellmer et al., 1999). Therefore, we consider their Sr isotopic uniformity to be a reflection of a primary petrogenetic characteristic, rather than a result of diffusive equilibration.

5.3. Comments on the OVC system

For MC-SIMS analyses of Kaharoa and Rotoma plagioclase crystals that have uniform An contents, we infer homogeneous Sr isotopic compositions to a high spatial resolution (12 μm) in individual crystals. This implies that An contents and Sr isotope ratios did not fluctuate dramatically during growth of these OVC crystals, and that open-system processes also did not vary significantly during the 9 ka interval between eruption of the two magmas studied. Previous investigations of recent, post-caldera OVC eruptions demonstrate that the intrusion of mafic magma, as evidenced by reversely zoned crystals and the presence of olivine and basaltic glass, triggered many of these eruptions, although pre-eruption interaction between rhyolites and basalts is limited due to the small volume of the intruder (e.g., Shane, 2015; Shane et al., 2008, 2007; Smith et al., 2004). Rims of plagioclase crystals analysed in this study reveal overall homogeneity, both isotopically ($^{87}Sr/^{86}Sr$ = 0.7056 ± 0.0001 among all analysed rims) and compositionally ($An_{30 \pm 7}$), and no evidence for interaction with mafic melts shortly prior to eruption. It may be that these crystals are not representative of the whole system. Since all analysed plagioclase crystals have rims that are normally-zoned and nearly identical in An contents, they may instead represent a portion of the system that is a buffered crystal mush, as has been suggested previously for Okataina and other felsic centres (Bachmann and Bergantz, 2004, 2008a, 2008b; Hildreth, 2004; Klemetti et al., 2011; Smith et al., 2005; Storm et al., 2012; Wilson and Charlier, 2016). However, it is also possible that the lack of An and isotopic variation along the rims of the plagioclase crystals implies more limited mixing between the intruder and resident magma than previously suggested.

The potential of basaltic intrusions serving as the primary trigger for

Table 3
Final corrected MC-SIMS analyses.

Plagioclase	Spot no.[a]	An	$^{87}Sr/^{86}Sr$	2σ	Plagioclase	Spot no.[a]	An	$^{87}Sr/^{86}Sr$	2σ
Kaharoa					Kaharoa continued				
KA2-1	37	39	0.7057	0.0008	KA3-6	210	24	0.7059	0.0008
	39	43	0.7051	0.0008		211	24	0.7055	0.0008
	40	38	0.7050	0.0008		212	21	0.7053	0.0008
	43	31	0.7055	0.0008		215	33	0.7057	0.0008
	44	36	0.7058	0.0008		336	33	0.7051	0.0008
	46	32	0.7056	0.0008		216	32	0.7056	0.0008
	48	21	0.7061	0.0008		337	32	0.7045	0.0008
KA2-2	49	71	0.7055	0.0009		340	32	0.7051	0.0008
	56	71	0.7056	0.0009		217	31	0.7055	0.0008
	128	67	0.7053	0.0009		223	28	0.7058	0.0008
	50	62	0.7059	0.0009		218	28	0.7062	0.0008
	132	62	0.7056	0.0009		338	28	0.7054	0.0008
	51	31	0.7055	0.0008		221	22	0.7055	0.0008
	129	31	0.7054	0.0008		219	22	0.7055	0.0008
	57	31	0.7058	0.0008		220	20	0.7050	0.0007
	131	28	0.7060	0.0008		222	20	0.7051	0.0007
	133	31	0.7056	0.0008	Rotoma				
	81	39	0.7055	0.0008	RM1-1	384	65	0.7039	0.0009
	52	29	0.7060	0.0008		385	58	0.7047	0.0009
	59	29	0.7057	0.0008		392	58	0.7045	0.0009
	84	31	0.7058	0.0008		386	51	0.7048	0.0008
	83	31	0.7060	0.0008		391	31	0.7056	0.0008
	86	31	0.7060	0.0008		387	43	0.7053	0.0008
	53	31	0.7065	0.0008		388	31	0.7055	0.0008
	88	25	0.7053	0.0008		390	31	0.7051	0.0008
	130	25	0.7059	0.0008		389	30	0.7054	0.0008
	85	25	0.7061	0.0008	RM1-2	403	52	0.7055	0.0008
KA2-3	135	60	0.7069	0.0009		404	53	0.7050	0.0008
	136	58	0.7071	0.0009		405	48	0.7052	0.0008
	137	58	0.7070	0.0009		406	37	0.7054	0.0008
	138	30	0.7065	0.0008		408	40	0.7056	0.0008
	134	34	0.7059	0.0008		409	37	0.7056	0.0008
	139	34	0.7055	0.0008	RM1-5	418	49	0.7058	0.0008
	140	29	0.7059	0.0008		419	36	0.7058	0.0008
	141	24	0.7060	0.0008		420	40	0.7058	0.0008
	142	26	0.7062	0.0008		421	35	0.7055	0.0008
	143	23	0.7062	0.0008		422	34	0.7059	0.0008
KA2-4	145	33	0.7055	0.0008		423	34	0.7059	0.0008
	146	38	0.7059	0.0008		424	34	0.7061	0.0008
	147	40	0.7062	0.0008		425	31	0.7057	0.0008
	148	34	0.7059	0.0008		426	31	0.7051	0.0008
	149	25	0.7059	0.0008		427	38	0.7052	0.0008
	203	25	0.7051	0.0008		428	49	0.7062	0.0008
	144	25	0.7063	0.0008		429	40	0.7056	0.0008
	150	26	0.7062	0.0008		430	37	0.7051	0.0008
	151	21	0.7052	0.0008	RM2-1	368	35	0.7045	0.0008
	152	21	0.7056	0.0008		369	30	0.7059	0.0008
	202	21	0.7043	0.0008		370	39	0.7055	0.0008
KA3-1	243	37	0.7060	0.0008		371	29	0.7056	0.0008
	244	38	0.7065	0.0008		372	36	0.7054	0.0008
	245	61	0.7058	0.0009		373	31	0.7054	0.0008
	246	53	0.7060	0.0008		374	31	0.7056	0.0008
	247	36	0.7057	0.0008		375	30	0.7052	0.0008
	248	33	0.7063	0.0008	RM3-1	346	29	0.7057	0.0008
	249	27	0.7058	0.0008		347	29	0.7058	0.0008
	250	21	0.7047	0.0007		348	34	0.7060	0.0008
KA3-2	214	26	0.7052	0.0008		349	34	0.7061	0.0008
	205	26	0.7056	0.0008		350	34	0.7059	0.0008
	206	26	0.7053	0.0008		351	32	0.7058	0.0008
	213	26	0.7051	0.0008		352	33	0.7056	0.0008
	207	25	0.7051	0.0008		353	41	0.7056	0.0008
	208	31	0.7058	0.0008		354	35	0.7059	0.0008
	209	33	0.7056	0.0008		355	38	0.7056	0.0008
	204	33	0.7053	0.0008		356	38	0.7051	0.0008

[a] SIMS spots are listed in order from core to rim.

eruption is especially pertinent for Kaharoa. Previous studies (Leonard et al., 2002; Nairn et al., 2004) suggest that multiple injections of primitive magma interacted with the silicic Kaharoa system prior to eruption. These studies suggested that the Kaharoa magma chamber was stratified, with three geochemically discrete rhyolitic magmas, which resulted in basalt intermingling with a limited part of the system (one magma situated at the base). Kaharoa plagioclase crystals analysed for isotopes were extracted from a unit interpreted to be isolated from the basalt injection until eruption (see Section 2). If these crystals do represent a buffered portion of the magma system, then Sr isotopic ratios are consistent with the aforementioned model where basalt interaction with the buffered portion of the system did not occur during

Table 4
Summary table of previously reported $^{87}Sr/^{86}Sr$ ratios in magmatic plagioclase ($CaAl2Si_2O_8$ to $NaAlSi_3O_8$).

Study	Method[a]	Sample location	$^{87}Sr/^{86}Sr$ maximum	$^{87}Sr/^{86}Sr$ minimum	$^{87}Sr/^{86}Sr$ Δ[b]	Precision[c]		Size[d]
Alves et al. (2009)	LA	Maua Granite Pluton, Brazil	0.71540	0.71040	0.0050	0.00070	2σ	160 (μm-d)
Arakawa et al. (1992)	TIMS	Miyakejima Volcano, Japan	0.70351	0.70341	*0.0001*	0.00002	2σ	(Whole)
Borges et al. (2014)	LA	Deccan Traps, India	0.71061	0.70968	0.0009	0.00016	2se	80 (μm-d)
Burns et al. (2015)	LA	Purico-Chascón Volcanic Complex, Chile	0.70900	0.70570	0.0033	0.00180	2se	65 (μm-d)
–	TIMS	Purico-Chascón Volcanic Complex, Chile	0.70890	0.70880	0.0001	0.00002	2se	65 (μm-w)
Chadwick et al. (2007)	TIMS	Merapi Volcano, Java, Indonesia	0.70628	0.70577	0.0005	0.00002	2σ	≥50 (μm-w)
Charlier et al. (2006)	TIMS	Parinacota Volcano, Chile	0.70690	0.70670	0.0002	0.00006	2se	≥50 (μm-w)
Charlier et al. (2007)	TIMS	Fish Canyon Tuff, Colorado, USA	0.70670	0.70630	0.0004	0.00002	2σ	≥50 (μm-w)
Charlier et al. (2008)	TIMS	Oranui/Taupo Caldera, New Zealand	0.70764	0.70553	0.0021	0.00006	2σ	≤300 (μm-d)
Christensen et al. (1995)	LA	Long Valley, California, USA	0.70629	0.70595	0.0003	0.00005	2σ	130 (μm-d)
Coote et al. (2018)	LA	Kaikohe-Bay of Islands, New Zealand	0.70580	0.70320	0.0026	0.00008	2σ	500 (μm-w)
Davidson and Tepley (1997)	TIMS	Chaos Crags, California, USA	0.704100	0.703700	0.0004	0.000005	2σ	500 (μm-w)
–	TIMS	Purico-Chascón Volcanic Complex, Chile	0.709200	0.706200	0.0030	0.000005	2σ	500 (μm-w)
–	TIMS	El Chichón Volcano, Mexico	0.705400	0.704500	0.0009	0.000005	2σ	≤300 (μm-d)
Davidson et al. (2001)	LA	El Chichón Volcano, Mexico	0.70630	0.70370	0.0026	0.00034	2σ	3–600 (ng)
Feldstein et al. (1994)	TIMS	San Vincenzo, Tuscany, Italy	0.71441	0.71355	0.0009	0.00005	2se	500 (μm-w)
Font et al. (2008)	TIMS	Skye Flood Basalts, UK	0.70530	0.70336	0.0019	0.00001	2σ	190 (μm-d)
Gao et al. (2015)	LA	Tengchong Volcanic Field, China	0.71380	0.70600	0.0078	0.00240	2σ	≥80 (μm-w)
Ginibre and Davidson (2014)	TIMS	Parinacota Volcano, Chile	0.70677	0.70659	0.0002	0.00003	2se	200 (μm-d)
Halama et al. (2002)	ICP-MS	Gardar Province, Greenland	0.70568	0.70369	0.0020	0.00011	2se	< 1000 (μm-w)
Kimura et al. (2013)	LA	Azuma Volcano, Japan	0.70474	0.70461	0.0001	0.00010	2se	10–20 (ng)
Lange et al. (2013)	TIMS	Various mid-ocean ridge basalts (MORB)	0.70374	0.70338	0.0004	0.00005	2σ	≥50 (μm-w)
Morgan et al. (2007)	TIMS	Stromboli Volcano, Italy	0.70648	0.70617	0.0003	0.00002	2σ	≥50 (μm-w)
Ramos and Reid (2005)	TIMS	Pisgah Cinder Cone, California, USA	0.70454	0.70429	0.0003	0.00001	2se	100 (ng)
Ramos et al. (2005)	LA	Columbia River Flood Basalts, USA	0.71277	0.71184	0.0009	0.00008	2se	≤160 (μm-d)
Ramos et al. (2004)	LA	Pisgah Cinder Cone, California, USA	0.70457	0.70429	0.0003	0.00009	2se	≤160 (μm-d)
Salisbury et al. (2008)	LA	Lassen Volcano, California, USA	0.70440	0.70398	0.0004	0.00018	2se	≤160 (μm-d)
Takahashi et al. (2013)	TIMS	Azuma Volcano, Japan	0.704712	0.704266	*0.0004*	0.000009	2σ	300 (μm-w)
–	LA	Azuma Volcano, Japan	0.70456	0.70394	0.0006	0.00005	2se	200 (μm-d)
Takahashi et al. (2006)	TIMS	Zao Volcano, Japan	0.70425	0.70420	0.00005	0.00002	2σ	7 (ng)
Tepley and Davidson (2003)	TIMS	Rum Layered Intrusion, Scotland	0.70518	0.70454	0.0006	0.00003	2σ	200 (μm-w)
Tepley et al. (1999)	TIMS	Chaos Crags, California, USA	0.70501	0.70378	0.0012	0.00007	2σ	≤800 (μm-w)
Tepley et al. (2000)	TIMS	El Chichon Volcano, Mexico	0.70522	0.70421	0.0010	0.00002	2σ	500 (μm-w)
Waight et al. (2002)	LA	Gardiner Intrusion, Greenland	0.70383	0.70373	0.0001	0.00002	2se	≤200 (μm-d)
Waight et al. (2000a)	ICP-MS	Lachlan Fold Belt, Australia	0.71163	0.70492	0.0067	0.00004	2σ	< 900 (μm-w)
Waight et al. (2000b)	ICP-MS	Lachlan Fold Belt, Australia	0.73276	0.73020	0.0026	0.00003	2σ	< 900 (μm-w)
Yang et al. (2013)	LA	Bushveld Complex, South Africa	0.70666	0.70506	0.0016	0.00042	2σ	≤200 (μm-d)

[a] LA refers to LA-MC-ICP-MS; ICP-MS refers to solution MC-ICP-MS.
[b] Variations in $^{87}Sr/^{86}Sr$ ratios represent single-crystal isotopic variations. If single-crystal variations were not available, ratios have been *italicized*.
[c] Precision listed in table is the lowest reported in the respective publication, or average if only average precision was reported.
[d] Size refers to: (1) LA-MC-ICP-MS diameter (μm-d), (2) TIMS microdrilled zone width (μm-w), (3) TIMS Sr amount (ng), or (4) TIMS entire crystal (whole).

plagioclase crystal growth. This supports a model where rejuvenation is mostly the product of heat and volatile transfer (e.g., Storm et al., 2014, 2012). Shane (2015) examined plagioclase from the same Kaharoa unit and observed greater textural and compositional variety among crystals than found in this study, although rims also displayed low-An normal zoning consistent with crystallization in a buffered, cool magmatic system. Notably, crystals with higher-An cores are present and could be derived from a basaltic component (Leonard et al., 2002; Shane, 2015). If these remnant cores are derived from injecting basalt, any interaction between the buffered rhyolitic systems and the basalt was minimal and allowed the system to return to equilibrium well before eruption. Alternatively, the compositional and isotopic uniformity of plagioclase rims suggest these cores may be relict (Shane, 2015).

Rotoma eruptives, like Kaharoa, exhibit mixing between two compositionally varied rhyolites (Smith et al., 2006, 2005). Specifically, Smith et al. (2006) present geochemical evidence for two individually homogeneous rhyolitic magmas that erupted and mixed to form a hybrid erupted unit. However, the authors point out that there is no geochemical indication for basalt influx and no petrographic evidence for mingling of Rotoma rhyolite magmas with mafic liquids, which is supported by plagioclase Sr isotopic ratios. The Rotoma eruption differs further from Kaharoa in that spatial evidence suggests that the two magmas were stored separately, with vents covering a length of 12 km (Smith et al., 2006). The lateral extent of the Rotoma eruption, tapping of two separately-stored magmas, and previous studies suggesting earthquakes and eruptions are linked at OVC (Berryman et al., 2008), imply that seismic activity could also be a potential trigger. Nonetheless, the ability of rhyolitic systems to remain active is dependent on system rejuvenation through addition of high-temperature mafic magma, and studies illustrate this is an especially important process at OVC (e.g., Nairn et al., 2004; Shane et al., 2008, 2007; Smith et al., 2004; Storm et al., 2014, 2012, 2011). However, lack of compositional and Sr isotopic variability in Rotoma plagioclase crystals imply that, if reactivation resulted from mafic influx, it was dominantly driven by heat and volatile transfer rather than mass (liquid) transfer between basalts and rhyolites.

Kaharoa and Rotoma plagioclase Sr isotopic compositions support similar sources for the Tarawera and Haroharo volcanic complexes, despite evidence for a complex system of magma storage and conduits at OVC, and regardless of their observed mineralogical differences (e.g., biotite in Kaharoa, cummingtonite in Rotoma; Leonard et al., 2002; Shane, 2015; Shane et al., 2007; Smith et al., 2006, 2005). Measured $^{87}Sr/^{86}Sr$ ratios fall between two isotopic endmembers – the Mesozoic metasedimentary Waipapa and Torlesse Composite Terranes and mantle-derived basalt (Gamble et al., 1993; Graham and Cole, 1991; McCulloch et al., 1994; Price et al., 2015). Specifically, these intermediate Sr isotope ratios indicate similar degrees of assimilation of metasediments with basalt (Smith et al., 2010, 2005). In addition, isotopic contrasts are subdued because the sources for the Mesozoic terranes are volcanic rocks and volcaniclastic materials from an arc environment (Price et al., 2015).

6. Conclusions

MC-SIMS allows for high-spatial resolution analysis of Sr isotopic compositions in plagioclase. Notably, the analytical uncertainty ca. ± 0.0008 of MC-SIMS makes this technique suitable for systems where $^{87}Sr/^{86}Sr$ isotopic variations at an intra-crystalline level are large (> 0.001). In such cases, fluctuations can be identified to significantly higher spatial resolution than previously possible. Sr isotopic analyses of young OVC plagioclase support an origin from similar sources for the two intra-caldera volcanic complexes, Tarawera and Haroharo. Furthermore, plagioclase compositional and isotopic ratios are consistent with contributions from mafic inputs, which have been shown to trigger eruptions at OVC, are likely dominated by heating and gas fluxing rather than mass transfer.

Acknowledgements

Support for this project came from the New Zealand Ministry of Business, Innovation, and Employment grant MAUX1507 to GFZ, the University of Auckland Postgraduate Research Student Support award to MS, and by Monka-sho grants to NK and HY.

Appendix A. Supplementary data

Supplementary data to this article can be found online at https://doi.org/10.1016/j.chemgeo.2019.03.016.

References

Alves, A., de Assis Janasi, V., Simonetti, A., Heaman, L.M., 2009. Microgranitic enclaves as products of self-mixing events: a study of open-system processes in the Maua Granite, Sao Paulo, Brazil, based on in situ isotopic and trace elements in plagioclase. J. Petrol. 50, 2221–2247. https://doi.org/10.1093/petrology/egp074.

Andrews, B.J., Gardner, J.E., Housh, T.B., 2008. Repeated recharge, assimilation, and hybridization in magmas erupted from El Chichón as recorded by plagioclase and amphibole phenocrysts. J. Volcanol. Geotherm. Res. 175, 415–426. https://doi.org/10.1016/j.jvolgeores.2008.02.017.

Arakawa, Y., Murakami, H., Kimata, M., Shimoda, S., 1992. Strontium isotope compositions of anorthite and olivine phenocrysts in basaltic lavas and scorias of Miyakejima volcano. Japan. J. Mineral. Petrol. Econ. Geol. 87, 226–239.

Bachmann, O., Bergantz, G.W., 2004. On the Origin of Crystal-poor Rhyolites: extracted from Batholithic Crystal Mushes. J. Petrol. 45, 1565–1582. https://doi.org/10.1093/petrology/egh019.

Bachmann, O., Bergantz, G.W., 2008a. The magma reservoirs that feed supereruptions. Elements 4, 17–21. https://doi.org/10.2113/GSELEMENTS.4.1.17.

Bachmann, O., Bergantz, G.W., 2008b. Rhyolites and their source mushes across tectonic settings. J. Petrol. 49, 2277–2285. https://doi.org/10.1093/petrology/egn068.

Berryman, K., Villamor, P., Nairn, I., van Dissen, R., Begg, J., Lee, J., 2008. Late Pleistocene surface rupture history of the Paeroa Fault, Taupo Rift, New Zealand. N. Z. J. Geol. Geophys. 51, 135–158. https://doi.org/10.1080/00288300809509855.

Bindeman, I.N., Davis, A.M., Drake, M.J., 1998. Ion microprobe study of plagioclase-basalt partition experiments at natural concentration levels of trace elements. Geochim. Cosmochim. Acta 62, 1175–1193. https://doi.org/10.1016/S0016-7037(98)00047-7.

Borges, M.R., Sen, G., Hart, G.L., Wolff, J.A., Chandrasekharam, D., 2014. Plagioclase as recorder of magma chamber processes in the Deccan Traps: Sr-isotope zoning and implications for Deccan eruptive event. J. Asian Earth Sci. 84, 95–101. https://doi.org/10.1016/j.jseaes.2013.10.034.

Budd, D.A., Troll, V.R., Deegan, F.M., Jolis, E.M., Smith, V.C., Whitehouse, M.J., Harris, C., Freda, C., Hilton, D.R., Halldórsson, S.A., Bindeman, I.N., 2017. Magma reservoir dynamics at Toba caldera, Indonesia, recorded by oxygen isotope zoning in quartz. Sci. Rep. 7, 40624. https://doi.org/10.1038/srep40624.

Burns, D.H., de Silva, S.L., Tepley, F., Schmitt, A.K., Loewen, M.W., 2015. Recording the transition from flare-up to steady-state arc magmatism at the Purico–Chascon volcanic complex, northern Chile. Earth Planet. Sci. Lett. 422, 75–86. https://doi.org/10.1016/j.epsl.2015.04.002.

Chadwick, J.P., Troll, V.R., Ginibre, C., Morgan, D., Gertisser, R., Waight, T.E., Davidson, J.P., 2007. Carbonate assimilation at Merapi Volcano, Java, Indonesia: insights from crystal isotope stratigraphy. J. Petrol. 48, 1793–1812. https://doi.org/10.1093/petrology/egm038.

Charlier, B.L.A., Ginibre, C., Morgan, D., Nowell, G.M., Pearson, D.G., Davidson, J.P., Ottley, C.J., 2006. Methods for the microsampling and high-precision analysis of strontium and rubidium isotopes at single crystal scale for petrological and geochronological applications. Chem. Geol. 232, 114–133. https://doi.org/10.1016/j.chemgeo.2006.02.015.

Charlier, B.L.A., Bachmann, O., Davidson, J.P., Dungan, M.A., Morgan, D.J., 2007. The upper crustal evolution of a large silicic magma body: evidence from crystal-scale Rb–Sr isotopic heterogeneities in the Fish Canyon magmatic system. Colorado. J. Petrol. 48, 1875–1894. https://doi.org/10.1093/petrology/egm043.

Charlier, B.L.A., Wilson, C.J.N., Davidson, J.P., 2008. Rapid open-system assembly of a large silicic magma body: time-resolved evidence from cored plagioclase crystals in the Oruanui eruption deposits, New Zealand. Contrib. Mineral. Petrol. 156, 799–813. https://doi.org/10.1007/s00410-008-0316-y.

Christensen, J.N., Halliday, A.N., Lee, D.-C., Hall, C.M., 1995. In situ Sr isotopic analysis by laser ablation. Earth Planet. Sci. Lett. 136, 79–85.

Cole, J.W., Deering, C.D., Burt, R.M., Sewell, S., Shane, P.A.R., Matthews, N.E., 2014. Okataina Volcanic Centre, Taupo Volcanic Zone, New Zealand: a review of volcanism and synchronous pluton development in an active, dominantly silicic caldera system. Earth-Sci. Rev. 128, 1–17. https://doi.org/10.1016/j.earscirev.2013.10.008.

Coote, A., Shane, P., Stirling, C., Reid, M., 2018. The origin of plagioclase phenocrysts in basalts from continental monogenetic volcanoes of the Kaikohe-Bay of Islands field, New Zealand: implications for magmatic assembly and ascent. Contrib. Mineral. Petrol. 173. https://doi.org/10.1007/s00410-018-1440-y.

Davidson, J.P., Tepley III, F.J., 1997. Recharge in volcanic systems: evidence from isotope profiles of phenocrysts. Science 275, 826–829.

Davidson, J.P., Tepley III, F.J., Knesel, K.M., 1998. Crystal isotope stratigraphy; a method for constraining magma differentiation pathways. Eos 79, 185–189.

Davidson, J., Tepley III, F.J., Palacz, Z., Meffan-Main, S., 2001. Magma recharge, contamination and residence times revealed by in situ laser ablation isotopic analysis of feldspar in volcanic rocks. Earth Planet. Sci. Lett. 184, 427–442.

Davidson, J.P., Morgan, D.J., Charlier, B.L.A., Harlou, R., Hora, J.M., 2007. Microsampling and isotopic analysis of igneous rocks: implications for the study of magmatic systems. Annu. Rev. Earth Planet. Sci. 35, 273–311. https://doi.org/10.1146/annurev.earth.35.031306.140211.

Dohmen, R., Faak, K., Blundy, J.D., 2017. Chronometry and speedometry of magmatic processes using chemical diffusion in olivine, plagioclase and pyroxenes. Rev. Mineral. Geochem. 83, 535–575. https://doi.org/10.2138/rmg.2017.83.16.

Eiler, J.M., Graham, C., Valley, J.W., 1997. SIMS analysis of oxygen isotopes: matrix effects in complex minerals and glasses. Chem. Geol. 138, 221–244.

Exley, R.A., 1983. Evaluation and application of the ion microprobe in the strontium isotope geochemistry of carbonates. Earth Planet. Sci. Lett. 65, 303–310.

Feldstein, S., Halliday, A., Davies, G., Hall, C., 1994. Isotope and chemical microsampling: constraints on the history of an S-type rhyolite, San Vincenzo, Tuscany. Italy. Geochim. Cosmochim. Acta 58, 943–958. https://doi.org/10.1016/0016-7037(94)90517-7.

Font, L., Davidson, J.P., Pearson, D.G., Nowell, G.M., Jerram, D.A., Ottley, C.J., 2008. Sr and Pb isotope micro-analysis of plagioclase crystals from Skye lavas: an insight into open-system processes in a flood basalt province. J. Petrol. 49, 1449–1471. https://doi.org/10.1093/petrology/egn032.

Gamble, J.A., Smith, I.E.M., McCulloch, M.T., Graham, I.J., Kokelaar, B.P., 1993. The geochemistry and petrogenesis of basalts from the Taupo Volcanic Zone and Kermadec Island Arc, SW Pacific. J. Volcanol. Geotherm. Res. 54, 265–290.

Gao, J.-F., Zhou, M.-F., Robinson, P.T., Wang, C.Y., Zhao, J.-H., Malpas, J., 2015. Magma mixing recorded by Sr isotopes of plagioclase from dacites of the Quaternary Tengchong volcanic field. SE Tibetan Plateau. J. Asian Earth Sci. 98, 1–17. https://doi.org/10.1016/j.jseaes.2014.10.036.

Giletti, B.J., Casserly, J.E.D., 1994. Strontium diffusion kinetics in plagioclase feldspars. Geochim. Cosmochim. Acta 58, 3785–3793.

Ginibre, C., Davidson, J.P., 2014. Sr isotope zoning in plagioclase from Parinacota Volcano (Northern Chile): quantifying magma mixing and crustal contamination. J. Petrol. 55, 1203–1238. https://doi.org/10.1093/petrology/egu023.

Ginibre, C., Wörner, G., Kronz, A., 2007. Crystal zoning as an archive for magma evolution. Elements 3, 261–266. https://doi.org/10.2113/gselements.3.4.261.

Graham, I.J., Cole, J.W., 1991. Petrogenesis of andesites and dacites of White Island volcano, Bay of Plenty, New Zealand, in light of new geochemical and isotopic data. N. Z. J. Geol. Geophys. 34, 279–294.

Halama, R., Waight, T., Markl, G., 2002. Geochemical and isotopic zoning patterns of plagioclase megacrysts in gabbroic dykes from the Gardar Province, South Greenland: implications for crystallisation processes in anorthositic magmas. Contrib. Mineral. Petrol. 144, 109–127. https://doi.org/10.1007/s00410-002-0388-z.

Hildreth, W., 2004. Volcanological perspectives on Long Valley, Mammoth Mountain, and Mono Craters: several contiguous but discrete systems. J. Volcanol. Geotherm. Res. 136, 169–198.

Houghton, B.F., Wilson, C.J.N., McWilliams, M.O., Lanphere, M.A., Weaver, S.D., Briggs, R.M., Pringle, M.S., 1995. Chronology and dynamics of a large silicic magmatic system: central Taupo Volcanic Zone, New Zealand. Geology 23, 13–16. https://doi.org/10.1130/0091-7613(1995)023<0013:CADOAL>2.3.CO;2.

Humphreys, M.C.S., Blundy, J.D., Sparks, R.S.J., 2006. Magma evolution and open-system processes at Shiveluch Volcano: insights from phenocryst zoning. J. Petrol. 47, 2303–2334. https://doi.org/10.1093/petrology/egl045.

Kawasaki, N., Kato, C., Itoh, S., Wakaki, S., Ito, M., Yurimoto, H., 2015. 26Al–26Mg chronology and oxygen isotope distributions of multiple melting for a Type C CAI from Allende. Geochim. Cosmochim. Acta 169, 99–114. https://doi.org/10.1016/j.gca.2015.07.037.

Kawasaki, N., Itoh, S., Sakamoto, N., Yurimoto, H., 2017. Chronological study of oxygen isotope composition for the solar protoplanetary disk recorded in a fluffy Type A CAI from Vigarano. Geochim. Cosmochim. Acta 201, 83–102. https://doi.org/10.1016/j.gca.2015.12.031.

Kennedy, A.K., Hutcheon, I.D., Wyllie, P.J., Wasserburg, G.J., 1990. Ion microprobe analysis of 87Sr/86 Sr in carbonates, in: Seventh International Conference on Geochronology. (Cosmochronology and Isotope Geology).

Kimura, J.-I., Takahashi, T., Chang, Q., 2013. A new analytical bias correction for in situ Sr isotope analysis of plagioclase crystals using laser-ablation multiple-collector

inductively coupled plasma mass spectrometry. J. Anal. At. Spectrom. 28, 945. https://doi.org/10.1039/c3ja30329b.
Klemetti, E.W., Deering, C.D., Cooper, K.M., Roeske, S.M., 2011. Magmatic perturbations in the Okataina Volcanic Complex. New Zealand at thousand-year timescales recorded in single zircon crystals. Earth Planet. Sci. Lett. 305, 185–194.
Lange, A.E., Nielsen, R.L., Tepley, F.J., Kent, A.J.R., 2013. Diverse Sr isotope signatures preserved in mid-oceanic-ridge basalt plagioclase. Geology 41, 279–282. https://doi.org/10.1130/G33739.1.
Leonard, G.S., Cole, J.W., Nairn, I.A., Self, S., 2002. Basalt triggering of the c. AD 1305 Kaharoa rhyolite eruption, Tarawera volcanic complex, New Zealand. J. Volcanol. Geotherm. Res. 115, 461–486. https://doi.org/10.1016/S0377-0273(01)00326-2.
Ludwig, K.R., 2003. User's manual for isoplot 3.00, a geochronlogical toolkit for Microsoft excel, in: Berkeley Geochronology Center Special Publication. p. 74.
McCulloch, M.T., Kyser, T.K., Woodhead, J.D., Kinsley, L., 1994. Pb-Sr-Nd-O isotopic constraints on the origin of rhyolites from the Taupo Volcanic Zone of New Zealand: evidence for assimilation followed by fractionation from basalt. Contrib. Mineral. Petrol. 115, 303–312.
Miller, J.A., Kent, A.J.R., 2009. The determination of maternal run time in juvenile Chinook salmon (Oncorhynchus tshawytscha) based on Sr/Ca and 87Sr/86Sr within otolith cores. Fish. Res. 95, 373–378. https://doi.org/10.1016/j.fishres.2008.09.030.
Morgan, D.J., Jerram, D.A., Chertkoff, D.G., Davidson, J.P., Pearson, D.G., Kronz, A., Nowell, G.M., 2007. Combining CSD and isotopic microanalysis: magma supply and mixing processes at Stromboli Volcano, Aeolian Islands. Italy. Earth Planet. Sci. Lett. 260, 419–431. https://doi.org/10.1016/j.epsl.2007.05.037.
Nairn, I.A., 2002. Geology of the Okataina Volcanic Centre. GNS Geologic Map 25.
Nairn, I.A., Self, S., Cole, J.W., Leonard, G.S., Scutter, C., 2001. Distribution, stratigraphy, and history of proximal deposits from the c. AD 1305 Kaharoa eruptive episode at Tarawera Volcano, New Zealand. N. Z. J. Geol. Geophys. 44, 467–484. https://doi.org/10.1080/00288306.2001.9514950.
Nairn, I., Shane, P., Cole, J., Leonard, G., Self, S., Pearson, N., 2004. Rhyolite magma processes of the ~AD 1315 Kaharoa eruption episode, Tarawera volcano, New Zealand. J. Volcanol. Geotherm. Res. 131, 265–294. https://doi.org/10.1016/S0377-0273(03)00381-0.
Nairn, I.A., Hedenquist, J.W., Villamor, P., Berryman, K.R., Shane, P.A.R., 2005. The ~AD1315 Tarawera and Waiotapu eruptions, New Zealand: contemporaneous rhyolite and hydrothermal eruptions driven by an arrested basalt dike system? Bull. Volcanol. 67, 186–193. https://doi.org/10.1007/s00445-004-0373-7.
Price, R., Mortimer, N., Smith, I., Maas, R., 2015. Whole-rock geochemical reference data for Torlesse and Waipapa terranes, North Island, New Zealand. N. Z. J. Geol. Geophys. 58, 213–228. https://doi.org/10.1080/00288306.2015.1026832.
Ramos, F.C., Reid, M.R., 2005. Distinguishing melting of heterogeneous mantle sources from crustal contamination: insights from Sr isotopes at the phenocryst scale, Pisgah Crater. California. J. Petrol. 46, 999–1012. https://doi.org/10.1093/petrology/egi008.
Ramos, F.C., Tepley III, F.J., 2008. Inter- and intracrystalline isotopic disequilibria: techniques and applications. Rev. Mineral. Geochem. 69, 403–443. https://doi.org/10.2138/rmg.2008.69.11.
Ramos, F.C., Wolff, J.A., Tollstrup, D.L., 2004. Measuring 87Sr/86Sr variations in minerals and groundmass from basalts using LA-MC-ICPMS. Chem. Geol. 211, 135–158. https://doi.org/10.1016/j.chemgeo.2004.06.025.
Ramos, F.C., Wolff, J.A., Tollstrup, D.L., 2005. Sr isotope disequilibrium in Columbia River flood basalts: evidence for rapid shallow-level open-system processes. Geology 33, 457. https://doi.org/10.1130/G21512.1.
Rosman, K.J.R., Taylor, P.D.P., 1998. Isotopic compositions of the elements 1997 (Technical Report). Pure Appl. Chem. 70, 217–235. https://doi.org/10.1351/pac199870010217.
Sahetapy-Engel, S., Self, S., Carey, R.J., Nairn, I.A., 2014. Deposition and generation of multiple widespread fall units from the c. AD 1314 Kaharoa rhyolitic eruption, Tarawera, New Zealand. Bull. Volcanol. 76. https://doi.org/10.1007/s00445-014-0836-4.
Salisbury, M.J., Bohrson, W.A., Clynne, M.A., Ramos, F.C., Hoskin, P., 2008. Multiple plagioclase crystal populations identified by crystal size distribution and in situ chemical data: implications for timescales of magma chamber processes associated with the 1915 Eruption of Lassen Peak. CA. J. Petrol. 49, 1755–1780. https://doi.org/10.1093/petrology/egn045.
Sano, Y., Shirai, K., Takahata, N., Amakawa, H., Otake, T., 2008. Ion microprobe Sr isotope analysis of carbonates with about 5μm spatial resolution: an example from an ayu otolith. Appl. Geochem. 23, 2406–2413. https://doi.org/10.1016/j.apgeochem.2008.02.027.
Scatena-Wachel, D.E., 1986. Ion Microprobe Measurements of Radiogenic Nuclides: Cosmochemical and Geochemical Tracers. University of Chicago, Department of Chemistry.
Shane, P.A.R., 2015. Contrasting plagioclase textures and geochemistry in response to magma dynamics in an intra-caldera rhyolite system, Okataina volcano. J. Volcanol. Geotherm. Res. 297, 1–10. https://doi.org/10.1016/j.jvolgeores.2015.03.013.
Shane, P.A.R., Martin, S.B., Smith, V.C., Beggs, K.F., Darragh, M.B., Cole, J.W., Nairn, I.A., 2007. Multiple rhyolite magmas and basalt injection in the 17.7 ka Rerewhakaaitu eruption episode from Tarawera volcanic complex, New Zealand. J. Volcanol. Geotherm. Res. 164, 1–26. https://doi.org/10.1016/j.jvolgeores.2007.04.003.
Shane, P.A.R., Nairn, I.A., Smith, V.C., Darragh, M., Beggs, K., Cole, J.W., 2008. Silicic recharge of multiple rhyolite magmas by basaltic intrusion during the 22.6 ka Okareka Eruption Episode, New Zealand. Lithos 103, 527–549. https://doi.org/10.1016/j.lithos.2007.11.002.
Singer, B.S., Dungan, M.A., Layne, G.D., 1995. Textures and Sr, Ba, Mg, Fe, K, and Ti compositional profiles in volcanic plagioclase: clues to the dynamics of calc-alkaline magma chambers. Am. Mineral. 80, 776–798.
Smith, V.C., Shane, P.A.R., Nairn, I.A., 2004. Reactivation of a rhyolitic magma body by new rhyolitic intrusion before the 15.8 ka Rotorua eruptive episode: implications for magma storage in the Okataina Volcanic Centre, New Zealand. J. Geol. Soc. 161, 757–772.
Smith, V.C., Shane, P.A.R., Nairn, I.A., 2005. Trends in rhyolite geochemistry, mineralogy, and magma storage during the last 50 kyr at Okataina and Taupo volcanic centres, Taupo Volcanic Zone, New Zealand. J. Volcanol. Geotherm. Res. 148, 372–406. https://doi.org/10.1016/j.jvolgeores.2005.05.005.
Smith, V.C., Shane, P.A.R., Nairn, I.A., Williams, C.M., 2006. Geochemistry and magmatic properties of eruption episodes from Haroharo linear vent zone, Okataina Volcanic Centre, New Zealand during the last 10 kyr. Bull. Volcanol. 69, 57–88. https://doi.org/10.1007/s00445-006-0056-7.
Smith, V.C., Shane, P.A.R., Nairn, I.A., 2010. Insights into silicic melt generation using plagioclase, quartz and melt inclusions from the caldera-forming Rotoiti eruption, Taupo volcanic zone, New Zealand. Contrib. Mineral. Petrol. 160, 951–971. https://doi.org/10.1007/s00410-010-0516-0.
Stern, T.A., 1987. Asymmetric back-arc spreading, heat flux and structure associated with the Central Volcanic Region of New Zealand. Earth Planet. Sci. Lett. 85, 265–276.
Storm, S., Shane, P.A.R., Schmitt, A.K., Lindsay, J.M., 2011. Contrasting punctuated zircon growth in two syn-erupted rhyolite magmas from Tarawera volcano: insights to crystal diversity in magmatic systems. Earth Planet. Sci. Lett. 301, 511–520. https://doi.org/10.1016/j.epsl.2010.11.034.
Storm, S., Shane, P.A.R., Schmitt, A.K., Lindsay, J.M., 2012. Decoupled crystallization and eruption histories of the rhyolite magmatic system at Tarawera volcano revealed by zircon ages and growth rates. Contrib. Mineral. Petrol. 163, 505–519. https://doi.org/10.1007/s00410-011-0682-8.
Storm, S., Schmitt, A.K., Shane, P.A.R., Lindsay, J.M., 2014. Zircon trace element chemistry at sub-micrometer resolution for Tarawera volcano, New Zealand, and implications for rhyolite magma evolution. Contrib. Mineral. Petrol. 167, 1000. https://doi.org/10.1007/s00410-014-1000-z.
Streck, M.J., 2008. Time scales of magmatic processes from modeling the zoning patterns of crystals. Rev. Mineral. Geochem. 69, 595–622. https://doi.org/10.2138/rmg.2008.69.14.
Takahashi, T., Yoshikawa, M., Shibata, T., Tatsumi, Y., Shimizu, N., 2006. Sr isotopic micro analyses of plagioclase in andesites from Zao Volcano. NE Japan. Front. Res. Earth Evol. 2, 1–5.
Takahashi, T., Hirahara, Y., Miyazaki, T., Senda, R., Chang, Q., Kimura, J.I., Tatsumi, Y., 2013. Primary magmas at the volcanic front of the NE Japan Arc: coeval eruption of crustal low-K tholeiitic and mantle-derived medium-K calc-alkaline basalts at Azuma Volcano. J. Petrol. 54, 103–148. https://doi.org/10.1093/petrology/egs065.
Tepley III, F.J., Davidson, J.P., 2003. Mineral-scale Sr-isotope constraints on magma evolution and chamber dynamics in the Rum layered intrusion. Scotland. Contrib. Mineral. Petrol. 145, 628–641. https://doi.org/10.1007/s00410-003-0481-y.
Tepley III, F.J., Davidson, J.P., Clynne, M.A., 1999. Magmatic interactions as recorded in plagioclase phenocrysts of Chaos Crags, Lassen Volcanic Center. California. J. Petrol. 40, 787–806.
Tepley III, F.J., Davidson, J.P., Tilling, R.I., Arth, J.G., 2000. Magma mixing, recharge and eruption histories recorded in plagioclase phenocrysts from El Chichon Volcano. Mexico. J. Petrol. 41, 1397–1411.
Ustunisik, G., Kilinc, A., Nielsen, R.L., 2014. New insights into the processes controlling compositional zoning in plagioclase. Lithos 200–201, 80–93. https://doi.org/10.1016/j.lithos.2014.03.021.
Valley, J.W., Kita, N.T., 2009. In situ oxygen isotope geochemistry by ion microprobe. MAC Short Course Second. Ion Mass Spectrom. Earth Sci. 41, 19–63.
Vroon, P.Z., van der Wagt, B., Koornneef, J.M., Davies, G.R., 2008. Problems in obtaining precise and accurate Sr isotope analysis from geological materials using laser ablation MC-ICPMS. Anal. Bioanal. Chem. 390, 465–476. https://doi.org/10.1007/s00216-007-1742-9.
Waight, T.E., Dean, A.A., Maas, R., Nicholls, I.A., 2000a. Sr and Nd isotopic investigations towards the origin of feldspar megacrysts in microgranular enclaves in two I-type plutons of the Lachlan Fold Belt, southeast Australia. Aust. J. Earth Sci. 47, 1105–1112. https://doi.org/10.1046/j.1440-0952.2000.00831.x.
Waight, Tod E., Maas, R., Nicholls, I.A., 2000b. Fingerprinting feldspar phenocrysts using crystal isotopic composition stratigraphy: implications for crystal transfer and magma mingling in S-type granites. Contrib. Mineral. Petrol. 139, 227–239. https://doi.org/10.1007/s004100000128.
Waight, T., Baker, J., Peate, D., 2002. Sr isotope ratio measurements by double-focusing MC-ICPMS: techniques, observations and pitfalls. Int. J. Mass Spectrom. 221, 229–244.
Wallace, L.M., Reyners, M., Cochran, U., Bannister, S., Barnes, P.M., Berryman, K., Downes, G., Eberhart-Phillips, D., Fagereng, A., Ellis, S., Nicol, A., McCaffrey, R., Beavan, R.J., Henrys, S., Sutherland, R., Barker, D.H.N., Litchfield, N., Townend, J., Robinson, R., Bell, R., Wilson, K., Power, W., 2009. Characterizing the seismogenic zone of a major plate boundary subduction thrust: Hikurangi Margin, New Zealand. Geochem. Geophys. Geosystems 10, n/a-n/a. doi:https://doi.org/10.1029/2009GC002610
Weber, P.K., Bacon, C.R., Hutcheon, I.D., Ingram, B.L., Wooden, J.L., 2005. Ion microprobe measurement of strontium isotopes in calcium carbonate with application to salmon otoliths. Geochim. Cosmochim. Acta 69, 1225–1239. https://doi.org/10.1016/j.gca.2004.05.051.
Wilson, C.J.N., Charlier, B.L.A., 2016. The life and times of silicic volcanic systems. Elements 12, 103–108. https://doi.org/10.2113/gselements.12.2.103.
Wilson, C.J.N., Rowland, J.V., 2016. The volcanic, magmatic and tectonic setting of the Taupo Volcanic Zone, New Zealand, reviewed from a geothermal perspective. Geothermics 59, 168–187. https://doi.org/10.1016/j.geothermics.2015.06.013.
Wilson, C.J.N., Rogan, A.M., Smith, I.E.M., Northey, D.J., Nairn, I.A., Houghton, B.F.,

1984. Caldera volcanoes of the Taupo volcanic zone, New Zealand. J. Geophys. Res. Solid Earth 89, 8463–8484.

Wolff, J.A., Ramos, F.C., Davidson, J.P., 1999. Sr isotope disequilibrium during differentiation of the Bandelier Tuff: constraints on the crystallization of a large rhyolitic magma chamber. Geology 27, 495–498.

Yang, S.-H., Maier, W.D., Lahaye, Y., O'Brien, H., 2013. Strontium isotope disequilibrium of plagioclase in the Upper Critical Zone of the Bushveld Complex: evidence for mixing of crystal slurries. Contrib. Mineral. Petrol. 166, 959–974. https://doi.org/10.1007/s00410-013-0903-4.

Zellmer, G.F., Blake, S., Vance, D., Hawkesworth, C., Turner, S., 1999. Plagioclase residence times at two island arc volcanoes (Kameni Islands, Santorini, and Soufriere, St. Vincent) determined by Sr diffusion systematics. Contrib. Mineral. Petrol. 136, 345–357.